Halo Coronal Mass Ejections and Configuration of the Ambient Magnetic Fields

Y. Liu[1]

ABSTRACT

In this study, we seek correlation between speed of the active region-related halo Coronal Mass Ejections (CMEs) and configuration of the ambient magnetic fields. Having studied 99 halo CMEs in the period from 2000 to 2004, we find that CMEs under the heliospheric current sheet are significantly slower than CMEs situated under unidirectional open field structures. The average speed of the former is 883 km/s, while the latter is 1388 km/s. The effect is not biased by the flare importance. This implies that the ambient magnetic field structure plays a role in determining speed of the halo CMEs.

Subject headings: Sun: solar activity—-Sun: coronal mass ejections— Sun: magnetic field structure

1. Introduction

This research follows our previous work (Liu and Hayashi 2006). In that work, we analyzed the active region-related fast halo Coronal Mass Ejections (CMEs) in October-November 2003. We found that these CMEs were associated with special structures of the ambient magnetic fields, and we concluded that these magnetic configurations play an additional role in ensuring a high speed for the fast halo CMEs when they propagate through the heliosphere, although the related flares' characteristics may determine the CMEs' speeds in the first place, as demonstrated in several current studies (Moon et al. 2002; Cheng et al. 2003; Zhang et al. 2004; Qiu et al. 2004). The magnetic field structure was computed from the synoptic maps of magnetic fields based on a Potential Field Source Surface model (PFSS) (Schatten et al. 1969; Altschuler and Newkirk 1969; Hoeksema et al. 1982; Wang and Sheeley 1992). In this model, it is assumed that the magnetic field is potential everywhere between the photosphere and a spherical source surface. The modeled field matches the radial component on the photosphere and is forced to become purely radial on the source surface.

---

[1]W. W. Hansen Experimental Physics Laboratory, Stanford University, Stanford, CA94305-4085

From the calculated fields, it is easy to identify three different magnetic configurations: coronal hole, heliospheric current sheet and plasma sheet. The heliospheric current sheet is the boundary between two open fluxes in the heliosphere with the opposite polarities (Schulz 1973; Wilcox et al. 1980), while the plasma sheet is the boundary of two open fluxes with the same polarity (Hundhausen 1972; Neugebauer et al. 2002, 2004; Zhao and Webb 2003). The halo CMEs can be classified based on locations of their solar sources in the calculated fields. Here we take the site of the associated flare for the source site of a halo CME. We denote a halo CME as type 1 CME if its solar source is under a heliospheric current sheet, type 2 if in an open flux area, and type 3 if under a plasma sheet. The fast halo CMEs in October-November 2003 are types 2 & 3 CMEs. This makes sense because the magnetic field configurations related to these types of CMEs are appropriate for a CME to propagate outward. That study suggests that the ambient magnetic fields play a role in determining CMEs' speed.

In this study, we extend that work using a statistical approach in order to reach a more general conclusion. First, we classify the halo CMEs, listed in the SOHO LASCO CMEs Catalog, into the three types. Next, we compare the speed distributions of these three samples. We argue that, statistically, the distributions should be the same if the ambient magnetic fields would not have influenced CMEs' speed. Here, the coronal/heliospheric magnetic field is computed from the synoptic maps of magnetic fields obtained by SOHO/MDI (Scherrer et al. 1995) or at the Wilcox Solar Observatory (WSO) based on the PFSS model.

The paper is organized as follows. The data used in this study is described in Section 2. The result is presented in Section 3. We conclude this research in Section 4.

2. Data and analysis

The halo CMEs used in this study are collected from various sources in order to avoid possible bias in determination of the CMEs' solar sources. The solar source of a halo CME discussed in this paper is a flare that is associated with this CME. First, we select halo CMEs from the SOHO LASCO CMEs Catalog, available on-line at *http://cdaw.gsfc.nasa.gov/CME_list/*. The selection criteria are (1) halo CME, and (2) identification of its solar source. The solar sources of the halo CMEs in this catalog are preliminarily determined by the LASCO operators by examining signatures shown in the EIT images, such as dimmings, localized brightenings and post-eruption loop arcades. 104 halo CMEs in the period from 2000 to 2004 are chosen. Second, we check solar source identification of these CMEs from other data including information from the Coordinated Data Analysis Workshop (CDAW) available on-line at *http://cdaw.gsfc.nasa.gov/geomag_cdaw/Data.html* (J. Zhang's table and D. Webb's

list), from J. Zhang's halo CMEs list (private communication, 2006), and also from publications (Zhang et al. 2003; Fazakerley et al. 2005; Gopalswamy et al. 2005; Kim et al. 2005; Moon et al. 2005; Williams et al. 2005; Zhou et al. 2006; Pohjolainen and Lehtinen 2006). These data can confirm 91 halo CMEs. For the rest of the 13 CMEs (most are in 2004), we check the solar sources following the criteria used by Zhang et al. (2003) and Yashiro et al. (2005). We first estimate the onset time of a halo CME by a first-order extrapolation of the CME trajectory to the solar disk center; we then search for any signatures, such as dimmings, localized brightenings, waves and post-eruption loop arcades, from the EIT data and the running difference images in a time window of one hour (30 minutes before and after the estimated onset time of the CME). In this way, we are able to confirm another 8 CMEs. The total halo CMEs used in this study is thus 99. Parameters of the associated flares are from the *Solar-Geophysical Data*.

We classify these halo CMEs into three types, as mentioned in Section 1. The coronal magnetic field is computed from synoptic maps of magnetic field from MDI or WSO based on the PFSS model. In the PFSS model, the source surface is set to be at a height of 2.5 solar radius (from solar center). To illustrate how a halo CME is classified and what the magnetic field looks like for each type of CMEs, we present in Figures 1-3 three examples, one for each type. This presentation of magnetic field configuration follows the way Zhao and Webb (2003) took in their article. Shown in the top panels of the Figures are synoptic maps of magnetic field from MDI data. Configuration of the coronal magnetic field computed from the PFSS model are exhibited in the middle and bottom panels. The middle panels show the locus of the computed heliospheric current sheet (thick black lines) and the locations of the footpoints of open field lines on the photosphere that correspond to the locations of coronal holes (dots). The colors represent different coronal holes. The small blue-red lines denote closed field lines from positive polarity (blue) to negative polarity (red). Only the closed fields below 1.25 solar radius (from the solar center) are plotted here. The bottom panels show the distribution of the magnetic field on the source surface that is situated at 2.5 solar radius. The different colors here represent the open field lines from the corresponding open field areas on the photosphere, as marked by the dots with the same color in the middle panels. The symbols of plus and minus represent positive and negative polarities, respectively. The thick black lines are the heliospheric current sheets. The locations of the active regions that were associated with the halo CMEs are marked by triangles in the middle and bottom panels. Figure 1 shows an example of type 1 CME. A halo CME, first seen in LASCO observation at 10:54 UT of 2000 July 14, was identified to be associated with a X5.7 flare occurred at 10:12 UT of July 14 in the active region AR9077. This region is under the heliospheric current sheet (the middle and bottom panels). We thus identify this CME as a type 1 CME. Exhibited in Figure 2 is a type 2 CME that was identified to be associated

with a X17.2 flare occurred at 11:10 UT of 2003 October 28 in the active region AR10486. This active region is in an open flux area (see middle and bottom panels). A type 3 CME, first seen from LASCO observation at 13:54 UT of 2003 November 11, is shown in Figure 3. This CME is identified to be associated with the 13:35 UT M1.6 flare in the active region AR10498. It is seen that this active region is under the boundary of two open areas with the same polarity (middle and bottom panels).

3. Results

Statistical properties of these halo CMEs are presented in Table 1. There is a small fraction of type 3 CMEs, while types 1 & 2 are roughly equal. The average speeds of type 2 and 3 CMEs appear to be significantly greater than that of type 1. A 95% confidence test clearly discriminates type 1 from types 2 & 3, but not for type 2 and type 3. Examining the configurations of the ambient magnetic fields, we can see that type 2 & 3 CMEs are actually associated with very similar magnetic structures: they are under the unidirectional open field structures. This may be the reason that the average speeds of types 2 and 3 are not significantly different. We therefore combine types 2 and 3 CMEs together hereafter. The average speed of types 2 & 3 is thus 1388 ± 629 km/s.

The speed distributions of the halo CMEs are presented in Figure 4. The black line histogram represents the speed distribution of type 1, and the dark histogram is for types 2 & 3. It is clear that, compared with type 1, types 2 & 3 have a speed distribution shifting toward high speed.

One task we need to do is to examine whether such distributions are biased by flare importance because it is suggested recently that the speed of CMEs is related to the characteristic of the associated flares (Moon et al. 2002; Cheng et al. 2003; Zhang et al. 2004; Qiu et al. 2004). Plotted in Figure 5 are distributions of flare class for these CMEs. The black line histogram is for type 1 CMEs, and the dark histogram is for types 2 & 3 CMEs. The distributions of flare class for these types of CMEs are very similar. This suggests that the difference of speed between type 1 and types 2 & 3 CMEs is not biased by flare importance. Thus we conclude that types 2 & 3 CMEs are faster than type 1.

4. Conclusions and discussions

We have examined 99 active region-related halo CMEs in the period from 2000-2004. We define three types of halo CMEs based on the locations of the solar sources of the CMEs

and the configurations of the ambient magnetic fields: the solar sources being under the heliospheric current sheets (type 1), in the open flux areas (type 2), and under the plasma sheets (type 3). We find that types 2 & 3 CMEs appear to be significantly faster than type 1. The effect is not biased by the flare importance. It implies that configuration of the ambient magnetic fields plays a role in determining halo CMEs' speed.

By examining the configurations of the ambient magnetic fields, we can see that types 2 & 3 are actually under unidirectional open magnetic structures while type 1 CMEs are situated under the heliospheric current sheets. This means that types 2 & 3 CMEs possess much less closed flux than type 1 that confines propagation of CMEs. This suggests that the overall closed field works as an additional role to shape propagation of a CME, although the associated flare may determine the speed of this CME in the first place, as shown in several current studies (Moon et al. 2002; Cheng et al. 2003; Zhang et al. 2004; Qiu et al. 2004). In fact, Chen (1996) has demonstrated the effect of the overlying field over a modeled flux rope that was erupted due to injection of the poloidal flux into the system. It is shown in that work that, during the initial eruption of a CME, the major forces withholding the motion are the gravity and the Lorentz force from the toroidal current in the flux rope and the background field. Closed flux in the background field thus functions to slow down the CME or even pull back the eruptive materials, leading to failure of the eruption (e.g. Ji et al. 2003). The viscous drag can also decelerate a CME, but only becomes dominant in late stages of the eruption after it propagates to a certain distance where the ambient solar wind can exert an important influence (Chen 1996; Vrsnak 2001). Such an influence is several orders less than the gravity and Lorentz force during initial eruption (Chen 1996).

REFERENCES

Altschuler, M. D., Newkirk, G., Jr. 1969, Sol. Phys., 9, 131

Chen, J. 1996, J. Geophys. Res., 101, 27499

Cheng, C. Z., Ren, Y., Choe, G. S., Moon, Y.-J. 2003, ApJ, 596, 1341

Fazakerley, A. N., Harra, L. K., Culhane, J. L., van Driel-Gesztelyi, L., Lucek, E., Matthews, S. A., Owen, C. J., Mazelle, C., Balogh, A., Reme, H. 2005, Geophys. Res. Lett., CiteID L13105

Gopalswamy, N., Yashiro, S., Liu, Y., Michalek, G., Vourlidas, A., Kaiser, M. L., Howard, R. A. 2005, J. Geophys. Res., CiteID A09S15

Hoeksema, J. T., Wilcox, J. M., Scherrer, P. H. 1982, J. Geophys. Res., 87, 10331

Hundhausen, A. J. 1972, Coronal Expansion and Solar Wind (New York: Springer)

Ji, H., Wang, H., Schmahl, E. J., Moon, Y.-J., Jiang, Y. 2003, ApJ, 595, L135

Kim, Y.-H., Moon, Y.-J., Cho, K.-S., Kim, K.-S., Park, Y. D. 2005, ApJ, 622, 1240

Liu, Y., Hayashi, K. 2006, ApJ, 640, 1135

Moon, Y.-J., Choe, G. S., Wang, Haimin, Park, Y. D., Gopalswamy, N., Yang, G., Yashiro, S. 2002, ApJ, 581, 694

Moon, Y.-J., Cho, K.-S., Dryer, M., Kim, Y.-H., Bong, Su-chan, Chae, Jongchul, Park, Y. D., 2005, ApJ, 624, 414

Neugebauer, M., Liewer, P. C., Smith, E. J., Skoug, R. M., Zurbuchen, T. H. 2002, J. Geophys. Res., 107, 1488

Neugebauer, M., Liewer, P. C., Goldstein, B. E., Zhou, X., Steinberg, J. T. 2004, J. Geophys. Res., 109, 10102

Pohjolainen, S., Lehtinen, N. J. 2006, A&A, 449, 359

Qiu, J., Wang, H., Cheng, C. Z., Gary, D. E. 2004, ApJ, 604, 900

Schatten, K. H., Wilcox, J. M., Ness, N. F. 1969, Sol. Phys., 6, 442

Scherrer, P. H., Bogart, R. S., Bush, R. I. et al. 1995, Sol. Phys., 162, 129

Schulz, M. 1973, *Astrophys. Space Science*, 24, 371

Vrsnak, B. 2001, Sol. Phys., 202, 173

Wang, Y. -M., Sheeley, N. R., Jr. 1992, ApJ, 392, 310

Wilcox, J. M., Hoeksema, J. T., Scherrer, P. H. 1980, *Science*, 209, 603

Williams, D. R., Torok, T., Demoulin, P., van Driel-Gesztelyi, L., Kliem, B. 2005, ApJ, 628, L163

Yashiro, S., Gopalswamy, N., Akiyama, S., Michalek, G., Howard, R. A. 2005, J. Geophys. Res., 110, CiteID A12S05

Zhang, J.; Dere, K. P.; Howard, R. A.; Bothmer, V. 2003, ApJ, 582, 520

Zhang, J., Dere, K. P., Howard, R. A., Vourlidas, A. 2004, ApJ, 604, 420

Zhao, X.P., & Webb, D. F., 2003, J. Geophys. Res., 108, 1234.

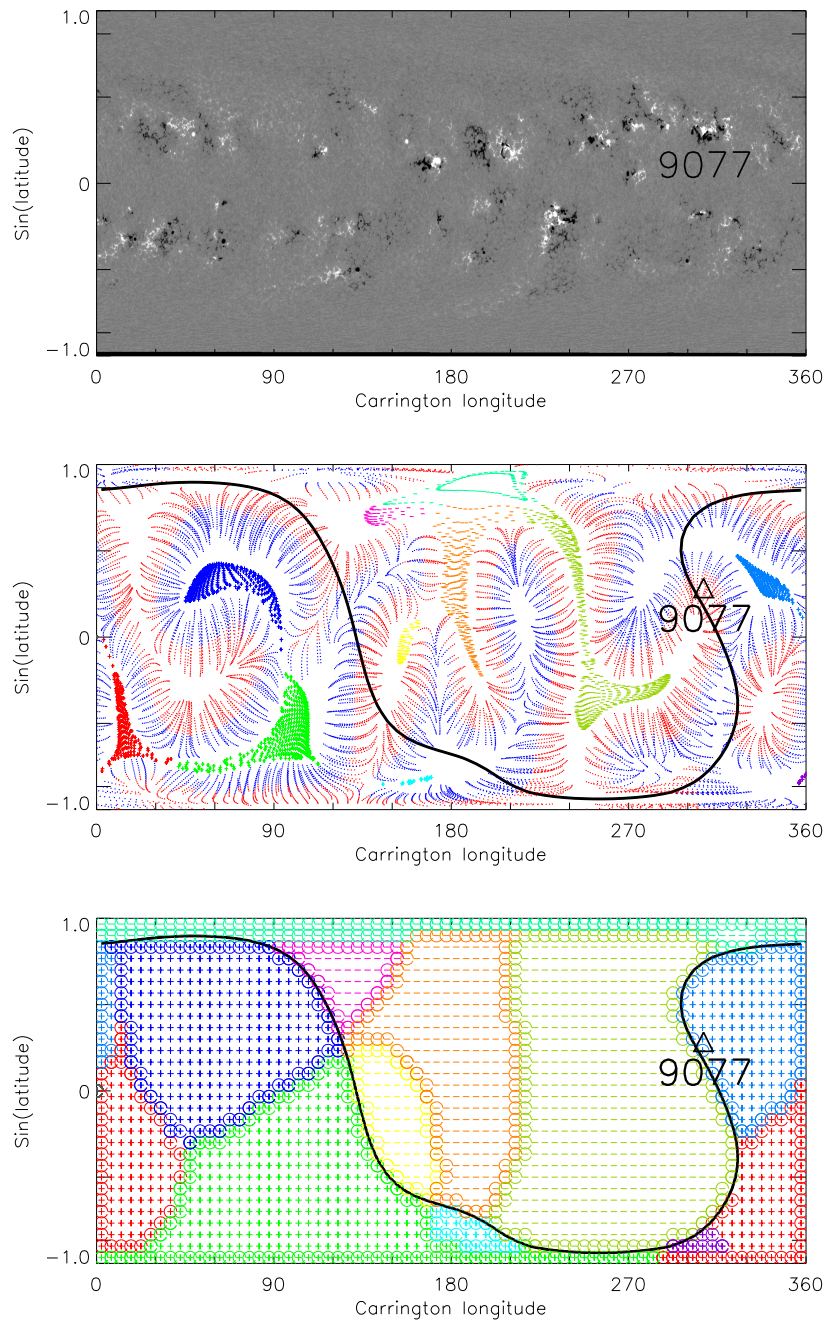Zhou, G. P., Wang, J. X., Zhang, J. 2006, A&A, 445, 1133

Fig. 1.— Configuration of the coronal magnetic field computed from the PFSS model for a type 1 CME. This halo CME, first seen in LASCO C2 observation at 10:54 UT of 2000 July 14, is identified to be associated with a X5.7 flare occurred at 10:12 UT of July 14 in the active region AR9077. Top panel: synoptic map of magnetic field from MDI magnetograms. Middle panel: the dots represent footpoints of open field lines on the photosphere. The small blue-red lines denote closed field lines from positive polarity (blue) to negative polarity (red). Only closed fields below 1.25 solar radius are plotted here. The thick black line represents the heliospheric current sheet. Bottom panel: the computed magnetic field on the source surface that is set to be at a height of 2.5 solar radius in the PFSS model. The different colors here denote the open field lines from the corresponding open field areas (marked by the dots with the same color in the middle panel) on the photosphere (at 1.0 solar radius). The symbols of plus and minus represent positive and negative fields, respectively. The thick black line is the heliospheric current sheet. The location of the active region AR9077 is marked as triangles in the middle and bottom panels.
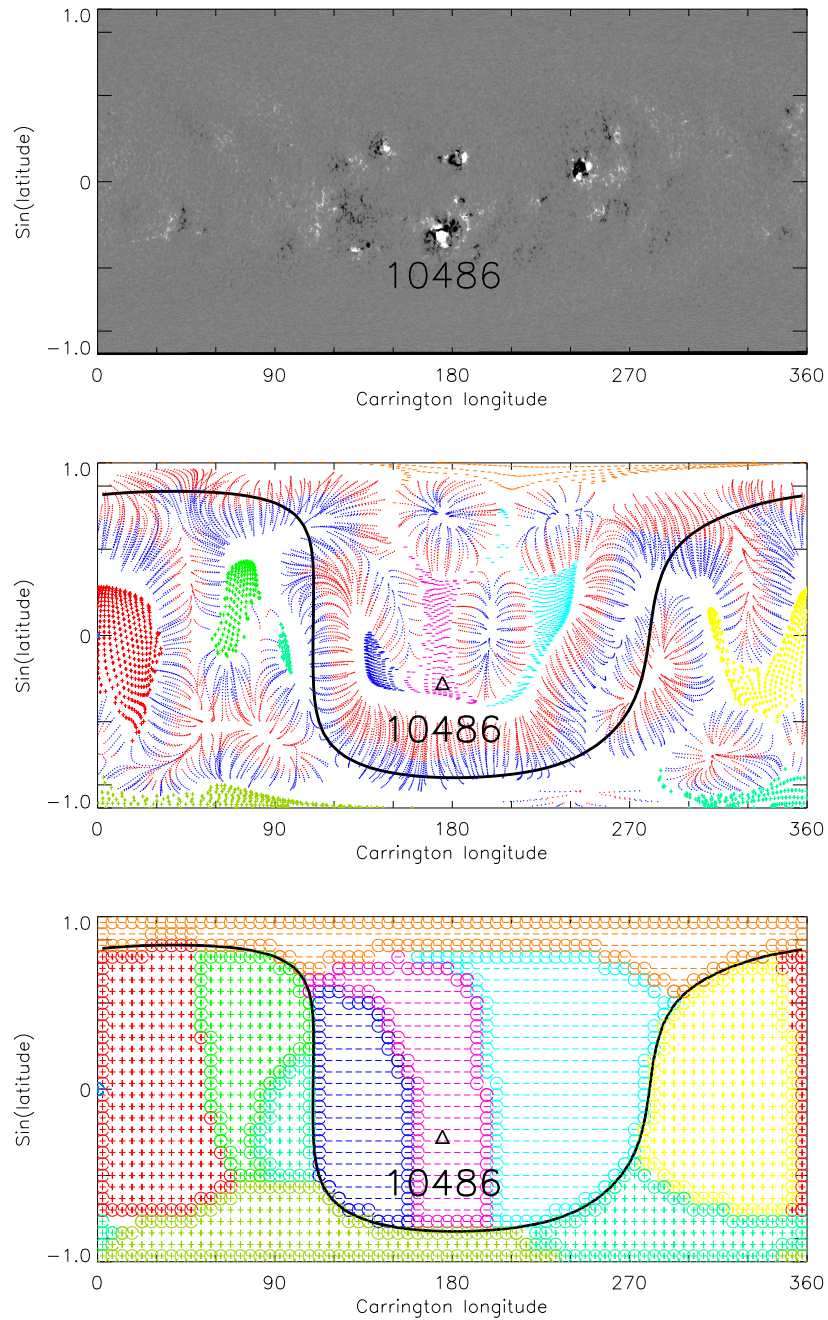
Fig. 2.— Same as Figure 1 but for a type 2 CME. This halo CME, first seen in the LASCO C2 image of 11:30 UT of 2003 October 28, is associated with a X17.2 flare occurred at 11:10 UT of October 28 in the active region AR10486.
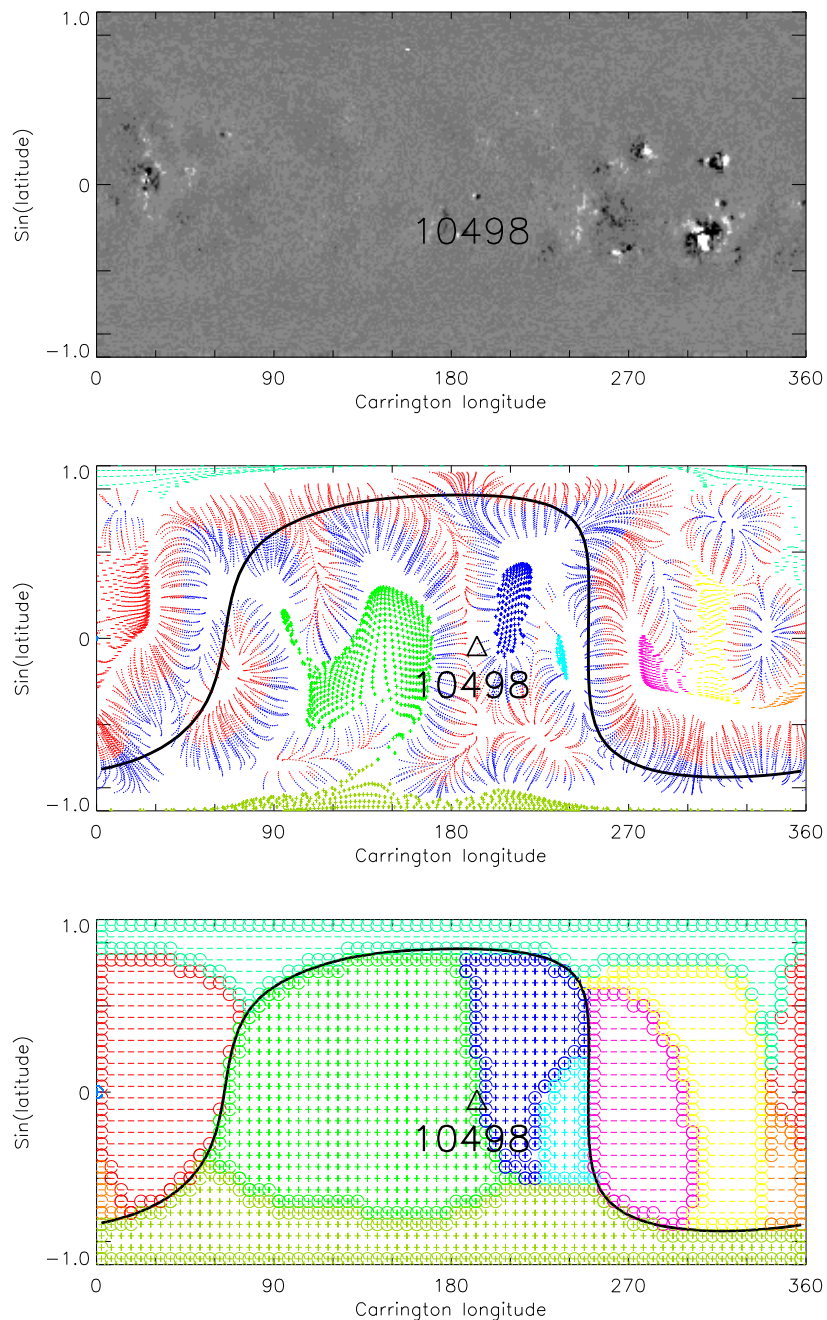
Fig. 3.— Same as Figure 1 but for a type 3 CME. This halo CME, first seen in the LASCO C2 image of 13:54 UT of 2003 November 11, is associated with a M1.6 flare at 13:35 UT of November 11 in AR10498.
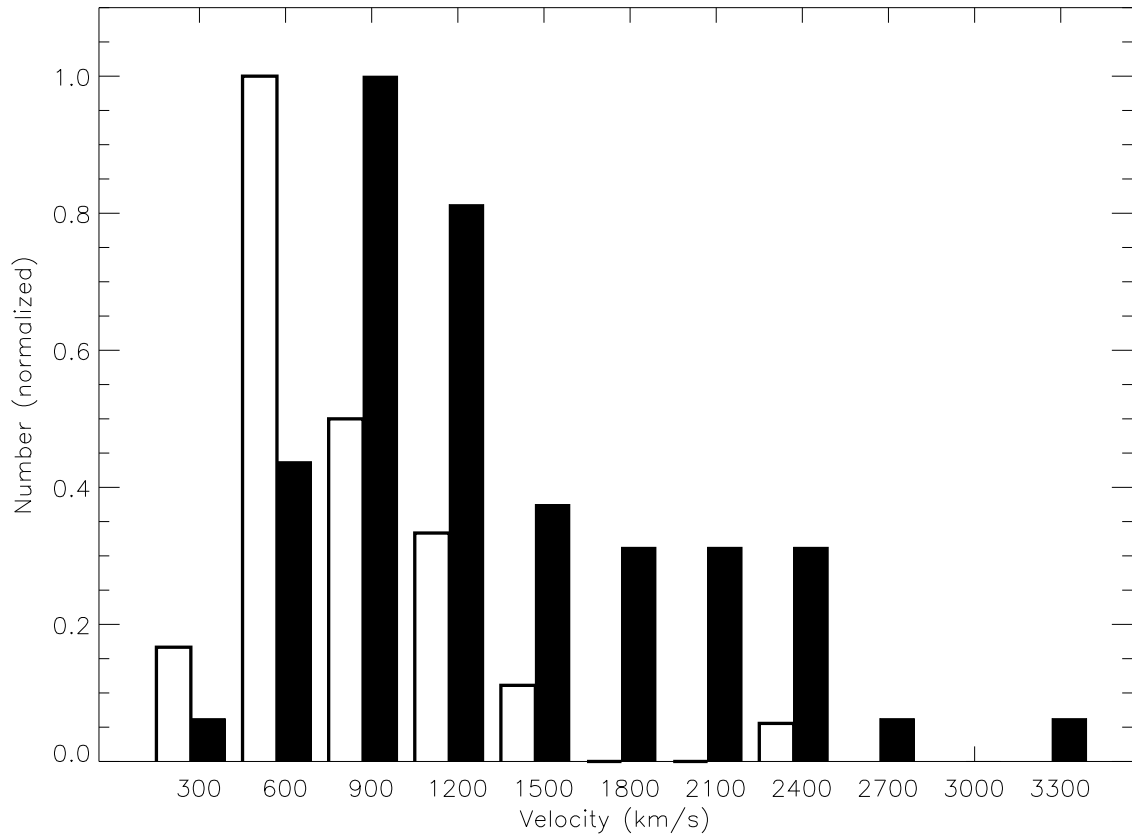
Fig. 4.— Speed distributions of the type 1 (black line histogram), and types 2 & 3 CMEs (dark histogram).
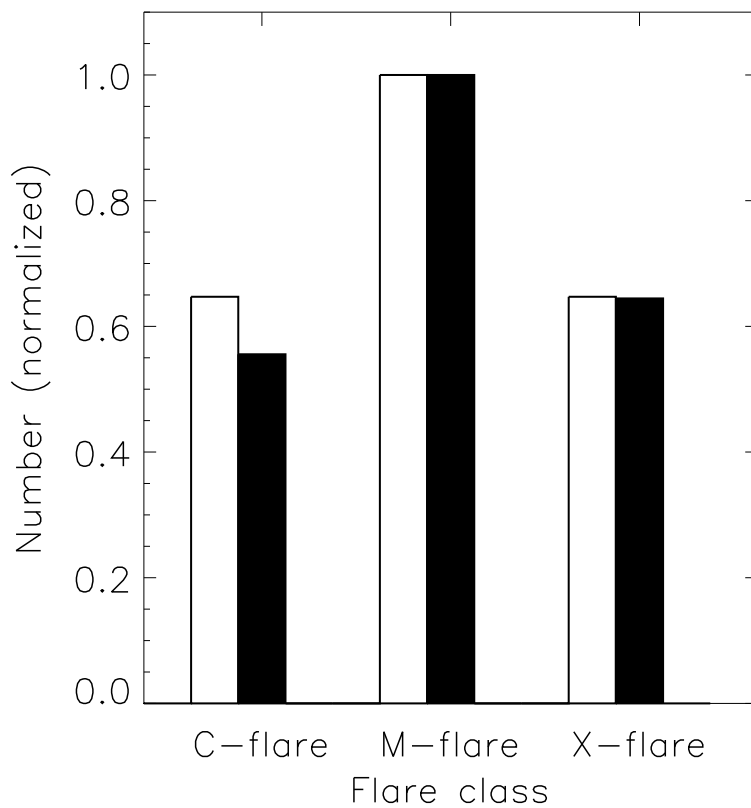
Fig. 5.— Distributions of the associated solar flares for type 1 (black line) and types 2 & 3 CMEs (dark).

Table 1: Statistical properties of the 99 halo CMEs from 2000 to 2004

	Type 1	Type 2	Type 3
Number	39	46	14
Percentage	39%	47%	14%
Median speed (km/s)	728	1208	1443
Mean speed (km/s)	883 ± 403	1345 ± 596	1530 ± 736